AAPS Open

RESEARCH

Open Access

Transdermal drug delivery system of lidocaine hydrochloride based on dissolving gelatin/sodium carboxymethylcellulose microneedles

Shabnam Bahmani[1], Ramin Khajavi[2*], Morteza Ehsani[1,3], Mohammad Karim Rahimi[4] and Mohammad Reza Kalaee[1]

Abstract

In this study, it was aimed to introduce a transdermal drug delivery system with dissolving microneedles (DMNs) based on gelatin (GEL) and sodium carboxymethyl cellulose (NaCMC) for lidocaine hydrochloride (LidoHCl) delivery. Different ratios of GEL and NaCMC were mixed, loaded with an active agent of LidoHCl, and treated with glutaraldehyde (GTA) as a crosslinker agent. Prepared hydrogels were cast into a silicon mold. Hereby, microneedles (MNs) with 500 µm height, 35° needle angle, 40-µm tip radius, and 960-µm tip-to-tip distance were fabricated. Samples containing LidoHCl 40%, GEL/NaCMC 5:1 (wt/wt), and polymer/GTA ratio 3.1 (wt/wt) showed the highest drug release ability ($t < 10$ min) with proper mechanical properties in comparison with other samples. Due to the drug release in a short time (fewer than 10 min), this drug delivery system can be used for rapid local anesthesia for pain relief as well as before minor skin surgeries.

Keywords Dissolving microneedles, Sodium carboxymethylcellulose/gelatin hydrogels, Lidocaine hydrochloride

*Correspondence:
Ramin Khajavi
rkhajavi@gmail.com; khajavi@azad.ac.ir
Full list of author information is available at the end of the article

Graphical Abstract

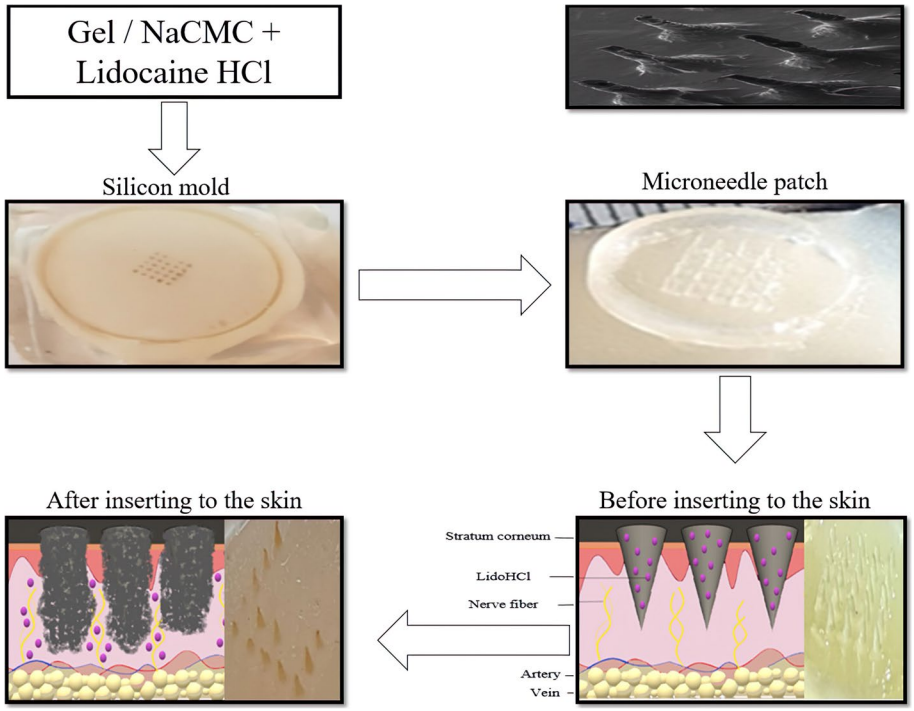

Introduction

The skin is the largest organ of the body that provides a convenient and accessible route for drug delivery (Han and Das 2015; Cevc and Chopra 2016). Transdermal drug delivery (TDD) demonstrates an attractive approach to systemic drug delivery and avoids pre-systematic metabolism (destruction in the gastrointestinal tract or by the liver), the possibility of controlled drug delivery for a long time, and an alternative solution for oral dosing in patients with anesthesia or nausea and direct access to the site or disease, for example, treatment of skin disorders such as fungal infections and psoriasis (Prausnitz MR and Langer R 2008; Jeong et al. 2021; Wang et al. 2021). Most importantly, since TDD is a noninvasive and almost painless administration method, it increases the acceptance of patients, especially children and the elderly (Inamuddin and Mohammad 2018; Zhu et al. 2001; Donnelly et al. 2012). However, there are several challenges to TDDs that have not yet fully achieved their potential as an alternative to hypodermic injections, mucosal administration, and oral delivery. First, the physicochemical properties of the skin create a barrier to drug delivery through the outermost layer of the skin epidermis called the stratum corneum (SC) (Jeong et al. 2021; Wang et al. 2021; Pastore et al. 2015). Second, only a limited number of drugs can be administered via TDDs (molecular weight less than 500 Da) (Bos and Meinardi 2000).

To overcome these limitations, an innovative microneedle (MN) approach aimed at developing safe and efficient means for delivering medications through the skin has attracted the attention of many scientists (Hao Y et al. 2017; Kochhar et al. 2016; Migdadi and Donnelly 2019; Ahmad et al. 2020; Bonfante et al. 2020; Liu et al. 2022; Dugam et al. 2021). DMNs penetrate the SC and dissolve in the interstitial tissue and release encapsulated drugs into the epidermal layer (He X et al. 2019; Bonfante et al. 2020; Ma and Wu 2017; Yang et al. 2020; Lee et al. 2020; Zhang et al. 2021; Xing et al. 2021). The evolution of these MNs has led to more innovative designs (Vecchione R. et al. 2014: Dugam et al. 2021; Vora et al. 2022; Roy et al. 2022; Shah and Choudhury 2017; Zhang et al. 2021). Hydrogel-forming MN or swellable MN can be used as a method developed from the "poke and release" approach for drug delivery (Liu et al. 2022; Li et al. 2018; Dash et al. 2013) due to their high water content, biodegradability, biocompatibility, and renewability (Bao et al. 2019; Ge et al. 2018). Among the local anesthetics, lidocaine is a frequently used medication for the treatment of chronic pain and acute (Zempsky WT 2008; Kochhar

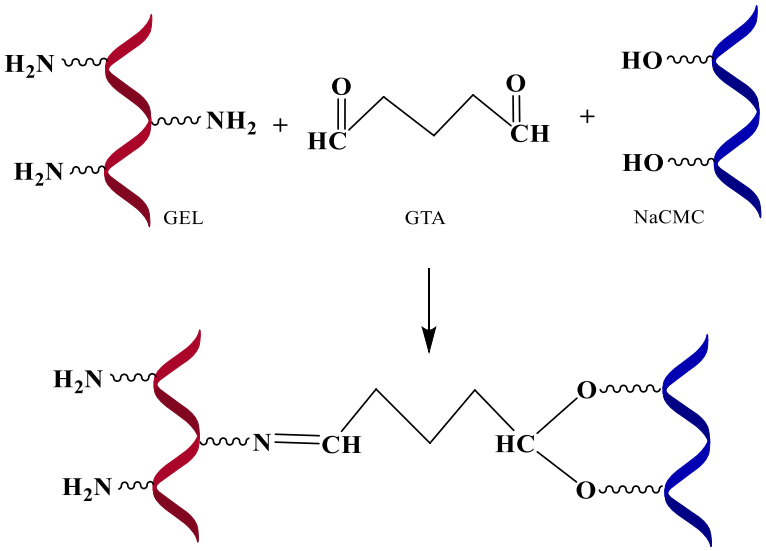

Fig. 1 The GEL/NaCMC hydrogel synthesis of schematic

et al. 2013; Gomes et al. 2016; Houck and Sethna 2005; Martell et al. 2017); lidocaine must get through a skin barrier to reach the nerve system in order to provide a local anesthetic (Gudin and Nalamachu 2020). Injectable Lido solution in either basic (lidocaine) or acidic forms (LidoHCl) has the mechanism of action antagonism of nerve signals in cells by inhibiting the influx of sodium ions through the sodium channels of the biological cell membrane, which response to temporary pain blockage on the skin surface (Rasool et al. 2020; Cepeda et al. 2015; Abdellatif and Ibrahim 2020). However, using syringes can cause anxiety, pain, and infection that lead to poor patient compliance and require a prescription by experienced medical personnel (Shin et al. 2017; Donnelly et al. 2010). Topical anesthetic gels and creams provide a simple, painless way to apply anesthesia. Nevertheless, these procedures lead to passive diffusion in the outer layer of the skin, resulting in slow-onset times of 30 to 60 min (Lee et al. 2020). This delayed onset is a major obstacle to the widespread use of local anesthetics for intravenous access methods (Donnelly et al. 2010; Spierings et al. 2008). To overcome this limitation, the MN has been studied to deliver drugs through the transdermal route for a fast onset time.

The use of biopolymers like polysaccharides and proteins for the crosslinking structure with the functional role of trapping drugs and with the goal of optimizing skin permeation pharmacokinetics has attracted the attention of many investigators (Santos LF et al. 2018; Edgar et al. 2021; Jeong et al. 2021; Mustafa Kamal et al. 2020). Gelatin (GEL) and sodium carboxymethyl cellulose (NaCMC) are biopolymers with bioavailability properties that can deliver therapeutic drugs transdermally as well as in combination with the composition of DNM (Nayak et al. 2013). GEL is a biodegradable protein that is naturally amphoteric due to the presence of both acidic and basic functional groups in the structure (Xing et al. 2014; Hajzamani et al. 2020). The low thermal and mechanical stability of GEL hydrogels has constrained their use in a variety of applications. However, by mixing GEL with other natural polymers such as NaCMC, and also using crosslinking agents such as glutaraldehyde (GTA), its thermal and mechanical stability can be improved (Khan and Anwar 2021; Liu et al. 2022; Favatela et al. 2021). GEL/NaCMC hydrogels can be modified according to the ratio of polymers and the amount of GTA for drug delivery under interstitial fluid conditions (pH = 5.5 and $T = 37$ °C). GEL/NaCMC hydrogel synthesis representation is given in Fig. 1. As the protein and polysaccharides utilized in this research include abundant amino and carboxyl groups, they generate a pH-sensitive hydrogel network. As per the literature, the interstitial fluid of the skin has a mildly acidic environment (Wagner et al. 2003; Proksch 2018; Ali and Yosipovitch 2013).

The literature review showed that there are not enough studies about dissolving microneedles for anesthetics drug delivery systems. Here, a DMN transdermal drug delivery system is proposed for the delivery of an anesthetic drug. GEL/NaCMC hydrogels in different mixing ratios were prepared and loaded with LidoHCl and crosslinked with glutaraldehyde. The structural characteristics of the DMN were determined by FTIR and XRD

to confirm the lack of chemical interactions between the drug and comprehend the polymers and the formation of crosslinking structure between GEL/NaCMC. The effect of varying concentrations of polymers, crosslinker, and amount of drug on swelling, solubility, gel fraction, drug release behavior, and mechanical strength was also evaluated. So, considering the highest swelling in skin conditions, we believed that the development of GEL/NaCMC hydrogels with MN morphology via a manner of "poke and release" is a promising approach for TDDs, and this strategy can be used for pain relief as well as before minor skin surgery, such as the removal of moles, warts, and verrucas.

Materials and methods

Materials

GEL type A (300 bloom), NaCMC (Mw 250 kDa, DS: 0.9), GTA solution (25% in water), and acetic acid were supplied from Sigma-Aldrich. LidoHCl (Mw 288.81 g mol^{-1}) was provided by Darou Pakhsh Pharma Chem. Co.. All chemicals were used without further purification.

Methods

Preparation of hydrogels

- Solution A: The clear gelatin solution was obtained by dispersing the required amount of GEL at 40 °C (Bello et al. 2020; Ivone et al. 2021) while stirring, and then, the required amount of LidoHCl was loaded into it (Table 1), and its pH was adjusted to 3.8–4.2 by adding acetic acid (0.1 M).
- Solution B: NaCMC was separately dispersed in distilled water and gently heated (~ 50 °C) to accelerate dissolution. Subsequently, solution B was added to solution A and stirred until a viscous solution was obtained. The total concentration of polymers in the solution was constant at 15 (w/v%) for all prepared samples. After cooling to 25 °C, the crosslinking agent (GTA) was added slowly under continuous stirring (400 rpm speed for 20 min).

Molding

Microneedle molds were made by a two-step "print and fill" method, using 3D printing (Krieger et al. 2019; Nejad et al. 2018). First, the positive template was designed using 3Design® software. Then, by examining the effects of MN mold geometry, the parameters of needle height (500 ± 10 µm), needle angle (35°), tip radius (40 ± 10 µm), and tip-to-tip distance (960 ± 10 µm) were optimized. The optimized design was printed using a 3D printer (DLP[1]). Afterward, it was washed with hot water and dried. The molding silicone resin with hardener (in a 10:1 ratio) was poured into the positive mold, and the procedure was completed by placing it in a vacuum oven overnight. The last negative silicone mold was used to create MN from hydrogels (Fig. 2).

Table 1 Formulation MNs

Sample codes	Mixing ratio GEL/NaCMC (wt/wt)	Polymer/GTA ratio (wt/wt)	LidoHCl content (%)
MN1	3:1	1.5	10
MN2	4:1	1.5	10
MN3	5:1	1.5	10
MN4	5:1	2.5	10
MN5	5:1	3.1	10
MN6	5:1	1.5	20
MN7	5:1	1.5	40

Scanning electron microscopy studies

The surface morphology of the DMN arrays was investigated using SEM (Vegall, Tescan). DMN samples were mounted on an aluminum mount and sputtered with a thin layer of gold. The samples were then placed into the SEM vacuum chamber and observed at various angles using an accelerating voltage of 15 kV. ImageJ software was used to measure the dimensions.

FT-IR spectroscopic analysis

FTIR spectral data were taken with the Infrared Bruker Tenso II instrument (at a resolution of 4 cm^{-1} and averaged 16 scans) to confirm the structure and also to find the chemical stability of the drug in the hydrogels. Gelatin, NaCMC, and LidoHCl were each separately finely grounded with KBr and thus kept ready for taking spectra. Also, for the GEL/NaCMC DMN and drug-loaded DMN, ATR spectroscopy was performed with an EQUINOX device from Bruker, Germany.

X-ray diffraction (XRD) analysis

X-ray pattern of LidoHCL, drug-loaded, and unloaded DMN was analyzed using Inel X-ray Diffractometer (EQUINOX 3000). This analysis was run at a current of 30 mA and voltage of 40 kV with Cu Ka radiation.

Swelling, solubility, and gel fraction

The swelling behavior of hydrogels in different pH values of 1.2, 5.5, 6.5, and 7.5 of USP phosphate buffers at 37 ± 0.1 °C was monitored (Khan and Anwar 2021). Typically, a certain amount (40 to 50 mg) of DMNs, dried to constant weight,

[1] Direct light processing

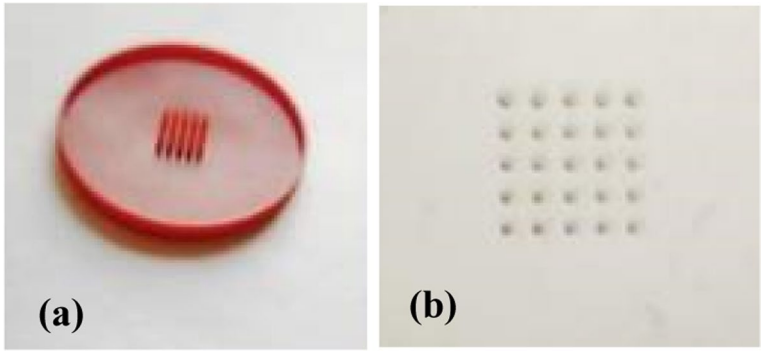

Fig. 2 MN mold. **a** Positive template fabricated by the 3D printer. **b** Obtained negative silicone mol

was placed in a pouch made of nylon cloth, weighted, and left to swell by immersing into a beaker containing the swelling media. At regular intervals, the pouch was removed from the solvent, after blotting with tissue paper to remove excess solvent on the surface, and was weighed using an electronic microbalance (Sartorius 313, accuracy of ± 0.01 mg) and then returned to the medium. The percentage of swelling determined at the time (t) was calculated using Eq. (1) (Saraswathy et al. 2020; Khan and Anwar 2021):

$$WR(\%) = \frac{Ws - Wd}{Ws} \times 100 \quad (1)$$

where W_s and W_d are the weights of swollen hydrogels at t, and dried hydrogels, respectively. The experiments were repeated three times and reported as a mean value.

The gel fraction was determined by weighing the unwashed DMNs before drying them in an oven at 40 °C (M_i). To remove non-crosslinked polymer, the samples were immersed in deionized water as a solvent for 24 h. After that, DMNs were dried in a vacuum oven at 40 °C until a constant weight was obtained (M_f). The percentage of gel fraction was calculated using Eq. (2) (Favatela et al. 2021):

$$GF(\%) = (\frac{Mf}{Mi}) \times 100 \quad (2)$$

Solubility analysis was performed to determine the quantity of partial dissolution or the percentage of mass lost. The DMNs were weighed before (M_i) and after (M_f) being placed in 100-ml buffer (PBS pH 5.5) at 37 °C for 48 h, and then, weight loss was inspected. The samples solubility was calculated based on Eq. (3) (Esteghlal et al. 2018):

$$\text{Solubility } (\%) = (M_i - M_f/M_i) \times 100 \quad (3)$$

Release study of LidoHCl in vitro

The in vitro drug release from LidoHCl-DMN was studied in PBS buffer (pH = 5.5) by dissolution analysis. For this purpose, the paddle-over disk method (Fig. 3) was used to examine the transdermal delivery systems (USP38/NF33 2015; Jesús et al. 2022; Price et al. 2020).

First, 500 ml of the buffer solution was poured into the vessel, and then, the DMN assembled on a disk was placed at the end of the vessel and stirred at 50 rpm. At predetermined time intervals, 2 ml of the solution was taken and replaced with a fresh one, and all samples were tested in triplicate. Sink conditions were maintained throughout the experiment, with the concentration of the LidoHCl in the release medium being less than 10% of the saturated solubility and constant temperature of 37 ± 0.5 °C. The concentration of LidoHCL in the release media was determined by UV–Vis spectrophotometer (PerkinElmer, LAMBDA 365, USA) at λ_{max} of 263 nm. To determine the reproducibility and the accuracy of the UV test, the RSD percentage was calculated, and it was determined to be less than 5%. Also, UV spectroscopy was performed for each of the ingredients of the formulation. Solution samples were tested separately, and PBS buffer (pH = 5.5) was the reference.

Calibration curve of LidoHCl

A calibration curve is required to determine the rate of drug release from the samples (Pandit et al. 2016; Kumar et al. 2012) Specified concentrations of LidoHCL (5, 10, 15, 20, 30, and 40 μg/ml) in the buffer (pH = 5.5) were scanned in the range of 200–400 nm by using a UV–Vis spectrophotometer, and a prominent peak was observed at 263 ± 1 (nm). The absorbance values were recorded at 263 nm with the corresponding concentrations, the calibration curve was plotted, and the line equation was obtained with $R^2 = 0.9953$. Using Eq. 4, the drug release rate was obtained by knowing its absorbance.

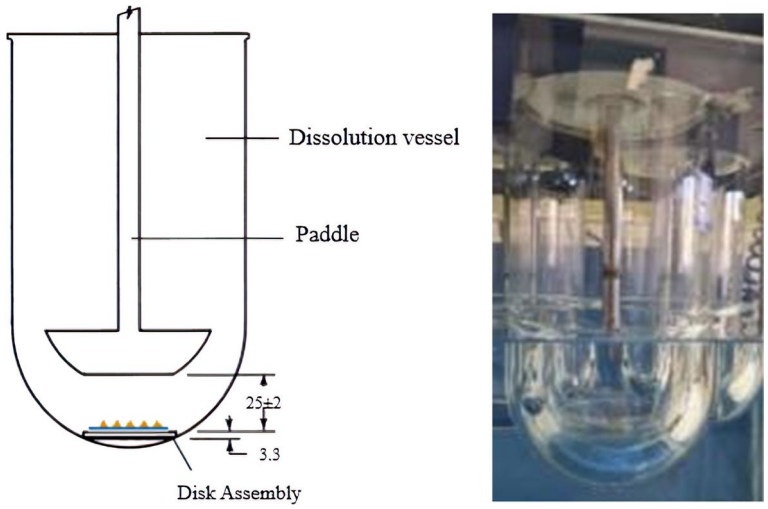

Fig. 3 Paddle over disk for dissolution test

$$\text{Absorbance} = 0.0181\,\text{Concentration}\,(\mu\text{g/ml}) + 0.0258 \quad (4)$$

Mechanical properties

The evaluation of the mechanical strength of the LidoHCl-DMN was measured using a SANTAM-STM20 instrument with a 6 N load cell as it allowed for sensitive measurements within an accuracy level of 0.4%. LidoHCl-DMNs containing 5×5 needle arrays were fixed on a platform surface under the vertically moving mechanical sensor using a double-sided adhesive tape. Then, the probe moved downward vertically at a speed of 0.5 mm s^{-1} as shown in Fig. 4. Subsequently, the varying force and sensor displacement were recorded during the test to obtain the axial force that causes the fracture of DMN.

Antibacterial analysis

The antimicrobial activities of the prepared MN were investigated using the diffusion method. One-hundred milliliters of gram-negative bacterial *Escherichia coli* and *Staphylococcus aureus* with a concentration of 0.5×10^7 was cultured, and it is used to test antibacterial activity by agar diffusion assay. The bacterial plates were placed in an incubator at 37 °C for 24 h. After 24 h, the plate was checked from the zone of inhibition by calculating the diameter of the inhibition section, and a picture was taken (Xue et al. 2013).

Results

Fabrication of MN

The polymer mixture was cast into the negative mold by centrifuged force. The negative silicon mold was first fitted at the end of the falcon tube, and then, the hydrogels were added and centrifuged for 5 min at 5000 rpm. The centrifugal force caused the hydrogels to enter the microcavities of the MN mold (Fig. 5e). The molds containing the hydrogel were then placed in a vacuum oven to dry for 6 h. Finally, the DMN hydrogels were

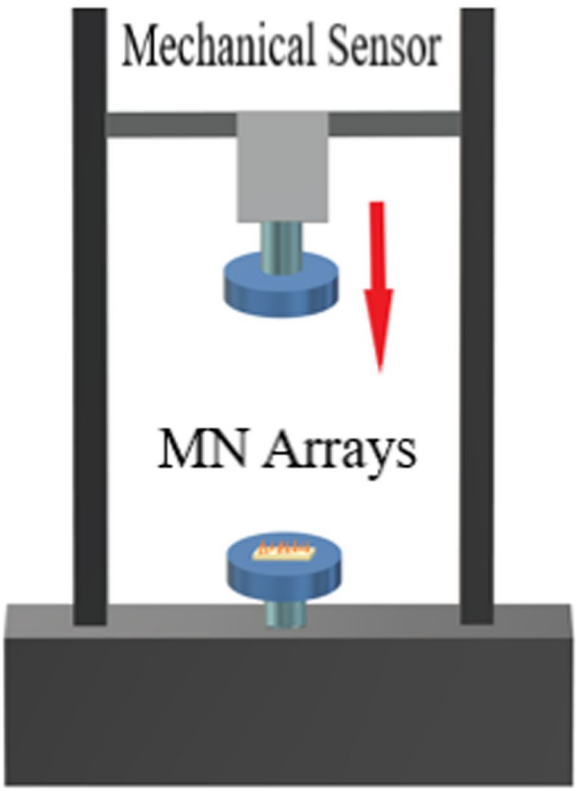

Fig. 4 Schematic of the mechanical test machine

separated from the mold and washed three times with distilled water (40 °C) to remove unreacted materials. The dried DMN hydrogels were placed in a vacuum-equipped desiccator until further usage.

Macrostructure

Figure 5a, b, and c indicated the surface morphology of DMN arrays. The DMN arrays in this study had a surface area of 25 (mm^2) and contained 25 MN equally distributed in a 5×5 arrangement (Fig. 5e, f). It was observed that SEM micrographs of the DMN arrays sample contain slightly rough surfaces. The structure of individual needles was evident at increased magnification (Fig. 5a).

Structure investigation

The ATR-FTIR analysis confirmed the successful crosslinking of GEL and NaCMC chains. The spectra of GEL, NaCMC, GEL/ NaCMC DMN, LidoHCl, and LidoHCl-loaded GEL/NaCMC DMN are presented in Fig. 6. As shown, the stretching vibrations of the O–H and N–H in the GEL/NaCMC hydrogel spectrum shifted gently to lower wavelengths. In addition, the amide I band shifted from 1654 to 1656 cm^{-1}. These indicated that the anionic groups in NaCMC with the cationic ones in GEL were coupled. On the other hand, the new bands in the range of 1150 to 1070 are attributed to the C–O–C stretching vibrations, which confirmed the crosslinking of the polymers.

Figure 7 shows the diffractograms of LidoHCl, Gel/NaCMC, and drug-loaded samples. As illustrated, LidoHCl has shown numerous characteristic sharp peaks due to its highly crystalline nature. The XRD pattern of blank GEL/NaCMC hydrogel (MNB sample) exhibits a broad peak, which represented the amorphous state. The diffractogram achieved by the drug-loaded GEL/NaCMC DMN (MN3, MN6, MN7) indicated the same amorphous state at $2 = \theta$ 21°. The appearance of peaks following LidoHCl loading at 14° and 26° indicates an increase in the crystallinity of the hydrogel samples.

Effects of pH, the ratio of polymers, and polymer/GTA ratio on swelling

The swelling behavior of GEL/NaCMC hydrogels is influenced by the pH of the immersed media, the ratio of the two polymers, and the amount of the crosslinking agent. Table 2 demonstrates the extent of the swelling of DMNs. The highest value of swelling was observed in acidic pH. Also, by raising the gelatin content in the microneedle composition, an increment in the water absorption of the microneedle was observed. The amount of glutaraldehyde had an inverse relation with swelling. In other words, increasing the crosslinker concentration forms a strong structure that declines the swelling.

Gel fraction and solubility study

The effects of the LidoHCl-DMN contents on the gel fraction are presented in Table 2. To scrutinize the effect of the amount of crosslink agent on GF%, three samples (MN3, MN4, and MN5) were studied with different amounts of polymer/GTA ratio (3.1, 2.5, and 1.5), while the ratio of polymers and the amount of drug are constant. These results show that increasing the amount of crosslink agent leads to an increase in the percentage of GF. To elaborate the effect of polymers ratio on GF of DMN, three samples (MN1, MN2, and MN3) were prepared with varying rates of GEL: NaCMC (3:1, 4:1, and 5:1) and keeping the amount of GTA and LidoHCl constant. This is because increasing the concentration of GTA leads to an increase in active sites for the crosslinking reaction. Thus, the crosslinking density between GEL and NaCMC increases, which leads to an increase in the mechanical strength of the hydrogel and a higher percentage of GF.

In vitro drug release

In vitro release studies were performed to understand drug release from LidoHCl-DMNs in the conditions of skin pH. The selectivity results revealed that in the λ_{max} of LidoHCl, each of the ingredients of the formulation had no significant absorption. As shown in Fig. 5g, h, and i, the tips of the needles swell after 5 min, and a significant amount of needles dissolve after 10 min. Figure 8 illustrates the effects of the ratio of the polymer, the amount of crosslinker, and the amount of medication on drug release at pH = 5.5.

Mechanical properties

An axial compression force was applied to the MN arrays to see whether they had adequate mechanical strength to penetrate the skin (Chen et al. 2021). As reported in the force/needle results of DMNs (Table 2), all MN arrays have the sufficient mechanical strength to penetrate the skin.

Antimicrobial activity

The prepared sample was applied to bacterial *E.coli* and *S.aureus* which results in antibacterial activity as shown in Fig. 9. MN7 proved to be antibacterial in nature. The average diameter of the zone of inhibition is 0.88 cm.

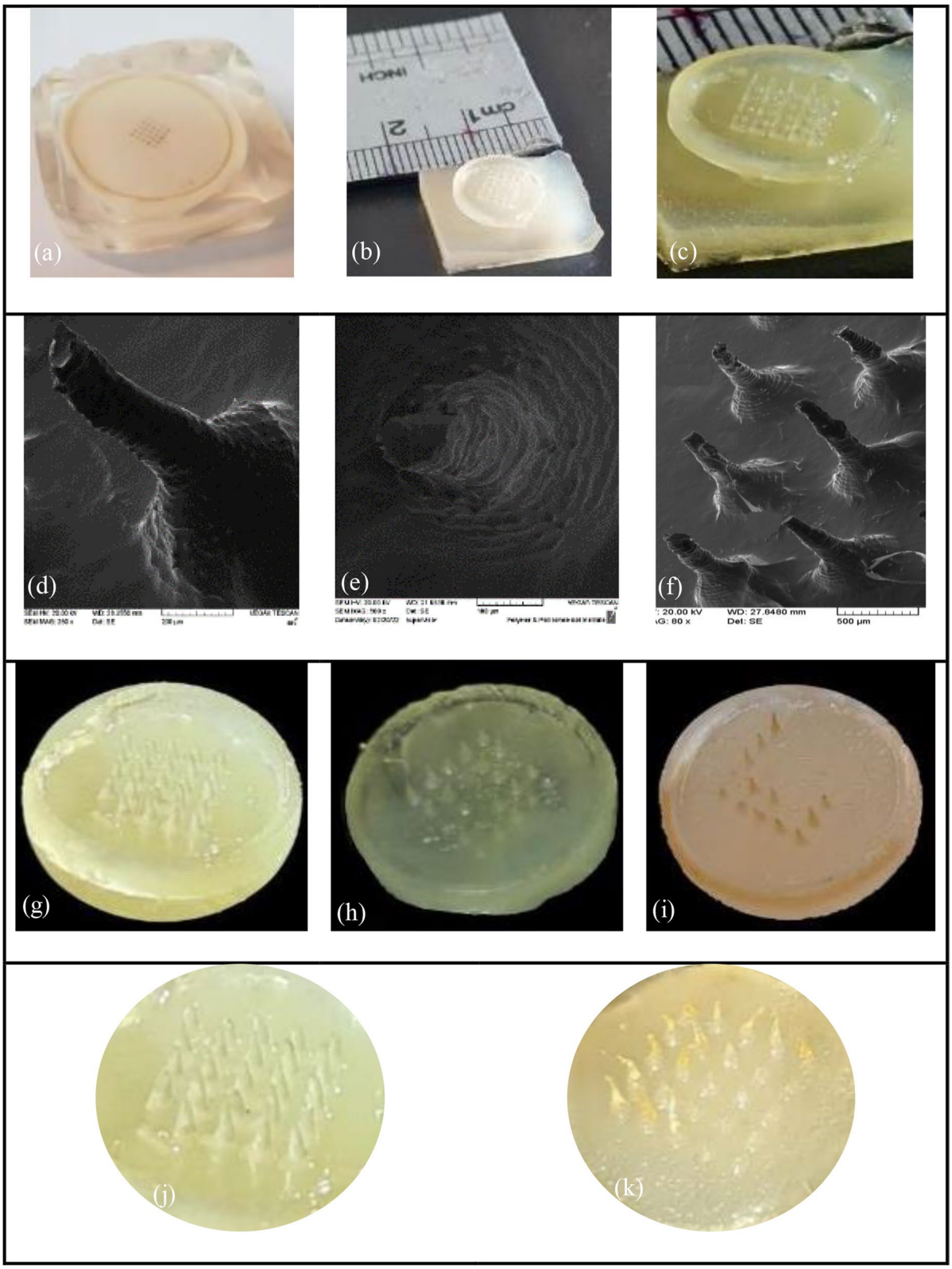

Fig. 5 LidoHCl DMNs. **a** Hydrogel-filled silicon mold. **b** and **c** Synthesized samples. **d** SEM at 280 × , **e** 500 × , **f** 80 × magnifications. **g** 0, **h** 5, and **i** 10 min after exposure to pH 5.5. **j** Before and **k** after the force application

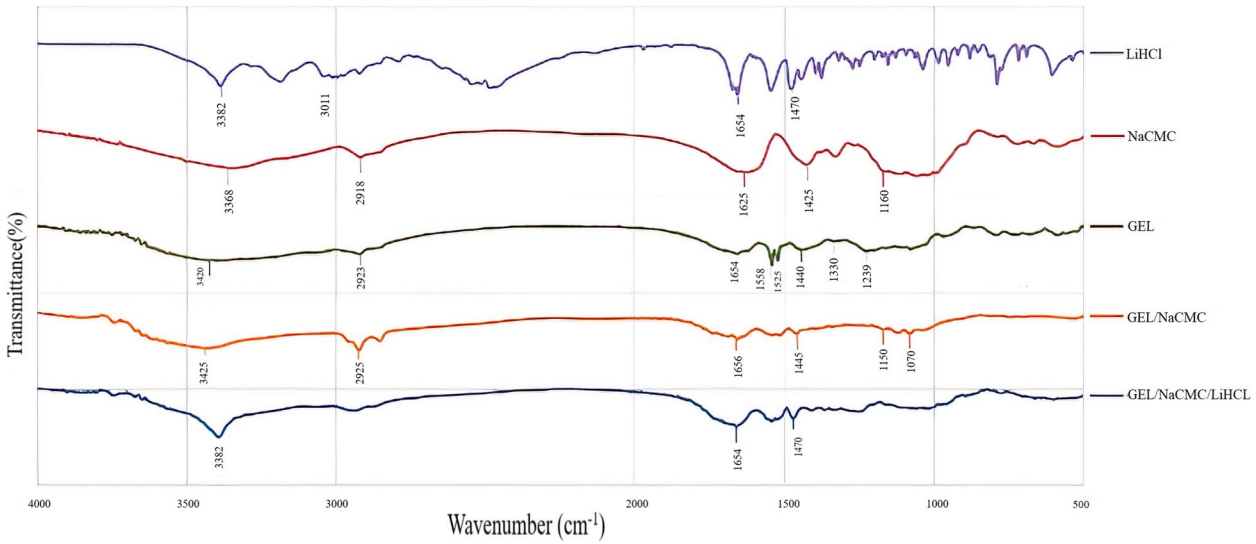

Fig. 6 FTIR spectra of the LidoHCL, NaCMC, GEL/NaCMC DMN, and drug-loaded DMN

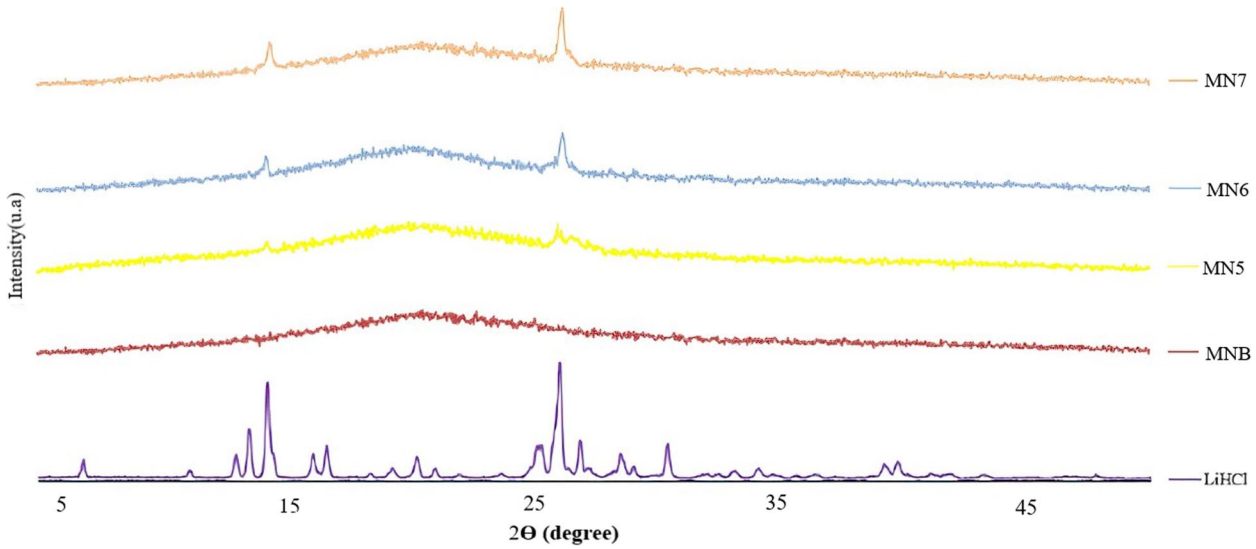

Fig. 7 XRD pattern of LidoHCl, MNB, MN3, MN6, and MN7 samples

Table 2 The results of swelling, GF, solubility, and mechanical strength tests

Sample codes	Degree of swelling (%)				GF (%)	Solubility (%)	Force/needle (*N*)
	pH (1.2)	pH (5.5)	pH (6.5)	pH (7.5)			
MN1	346	298	165	86	73	53	0.23
MN2	540	467	303	101	68.4	65	0.19
MN3	610	553	333	120	64.2	73	0.15
MN4	330	263	111	86	76.1	45	0.34
MN5	160	123	103	74	84.5	40	0.45
MN6	646	555	340	135	57	85	0.14
MN7	650	560	350	150	58.3	89	0.16

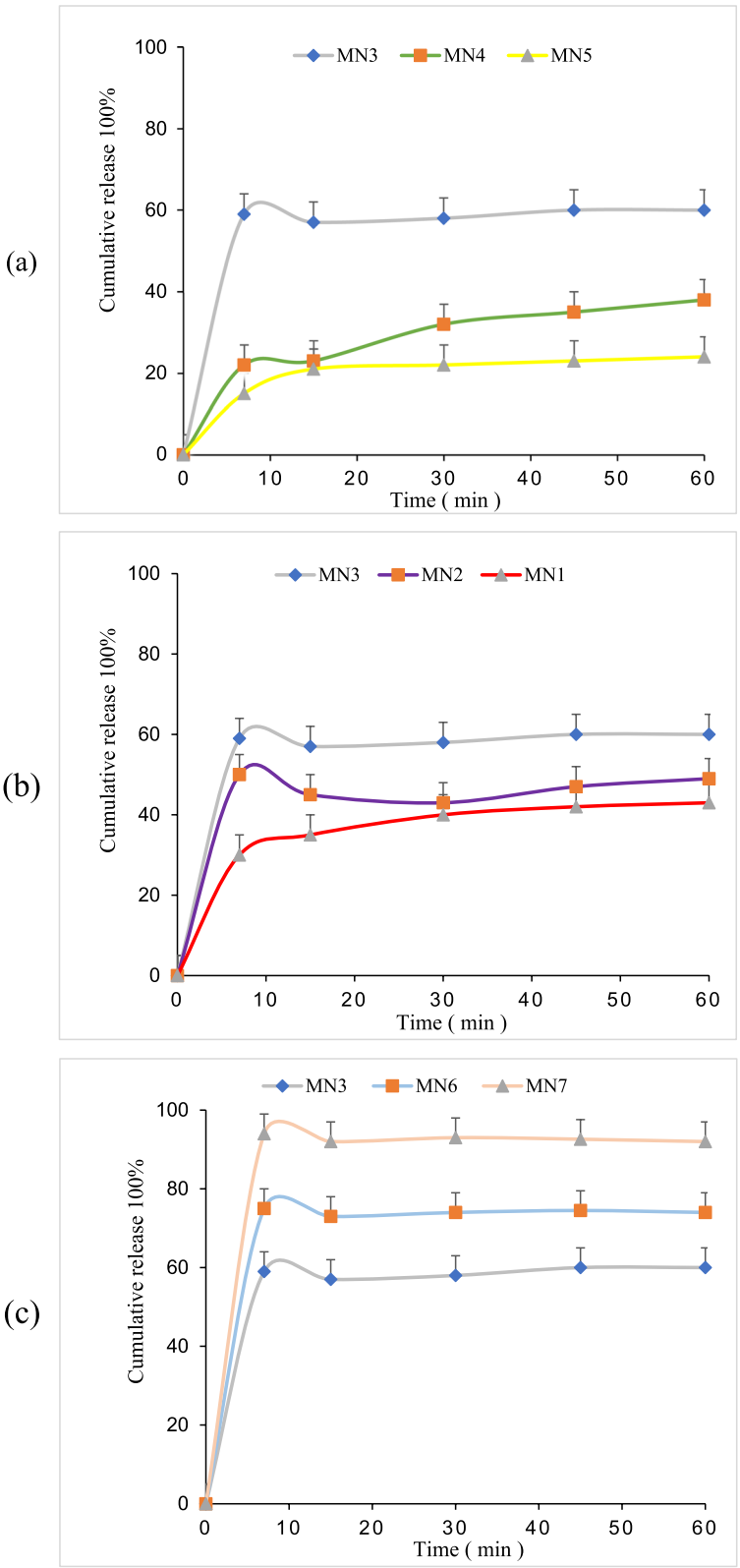

Fig. 8 Effect of **a** GTA, **b** polymer ratio, and **c** the amount of LidoHCl on in vitro release profile

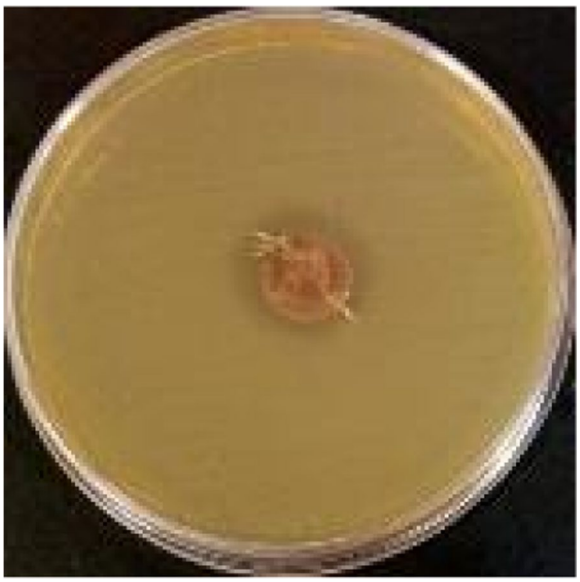

Fig. 9 Antimicrobial activity of MN7

Discussion

Dissolving and hydrogel-forming MN with the "poke and release" approach are a novel method of TDDs in which drugs can be loaded and released when the MN dissolves after insertion (Liu et al. 2022), also reducing onset time and improving permeability (Ma and Wu 2017; Yang et al. 2020). In this study, a mixture of a polysaccharide (NaCMC) and a protein (GEL) was used to create a drug delivery carrier with microneedle morphology. The dimensions of the prepared microneedle were needle height 450 µm, tip radius 30 µm, and tip-to-tip distance 960 µm. Examining the different dimensional parameters of the microneedle, it was found that needles with an input height of 300 to 600 µm are not of sufficient quality for molding, and higher heights may cause pain in the patient (Krieger et al. 2019; Nejad et al. 2018).

The ATR-FTIR spectrum of samples clearly showed the absorption bands of the crosslinked mixture of polymers. In the spectrum of GEL, a sharp absorbance band was observed at 3420 cm^{-1} due to N–H stretching vibration. The medium peak at 1558 cm^{-1} belonged to the N–H bending vibration. The absorption bands appearing at 1654 and 1330 cm^{-1} indicated the type 1 amide band and the C–N band stretching vibrations, respectively, which are the most significant peaks for FTIR analysis of the gelatin structure (Khan and Anwar 2021; Buhus et al. 2009). The medium peak at 1239 cm^{-1} belonged to the type 3 amide, and the weak peak that appeared at 1525 cm^{-1} was assigned to the type 2 amide. The band appearing at 1440 cm^{-1} indicated aliphatic C–H bending vibrations, while aliphatic C–H stretching vibrations were observed at 2923 cm^{-1}.

NaCMC showed a strong absorbance band at 3368 cm^{-1} was assigned to the O–H stretching vibration. The shoulder at 2918 cm^{-1} indicated aliphatic C–H stretching vibrations, while the strong peak at 1625 cm^{-1} and medium peak at 1425 cm^{-1} were due to the asymmetric and symmetric stretching of the carboxylate group. The intense peak of C–O stretching vibration for ethers was ascribed to the significant absorption peaks at 1000–1160 cm^{-1}. These findings are in good accord with findings from previous investigations (Devi and Maji 2009).

The main absorption peaks of LidoHCl powder were observed at 3382, 3011, 1654, and 1470 cm^{-1}. These bands were assigned as N–H stretching, C–H stretching, amide I (C = O), and amide II (C–N), respectively. FTIR spectra were also used to affirm the chemical stability of LidoHCL in samples. As observed in Fig. 6, the position of these bonds in drug-containing hydrogels almost remained unchanged, indicating there was no significant chemical interaction between the drug and the GEL/NaCMC hydrogels. It may be noted that in the case of drug-containing DMNs, the band observed at 1654 cm^{-1} overlapped with the GEL amide band, so XRD analysis was performed to confirm the stability of Lido in the hydrogel.

The intensity of XRD peaks was more noticeable for the MN7 sample than for the MN3 and MN6 samples, indicating a higher amount of drug. These results are consistent with the in vitro drug release data.

The study of swelling results showed that acidic media is due to the protonation of the free amino groups of GEL, which leads to electrostatic repulsions between them and thus expands the polymer network, whereas free carboxylic groups with hydroxyl groups of NaCMC may lead to a contraction of the network by intense hydrogen interactions or by intermolecular lactonization (Khan and Anwar 2021; Tataru et al. 2011). As the pH increases towards the basic medium, carboxylic groups of CMC become ionized, and GEL owns $COO-$ groups, and the electrostatic repulsion between the carboxylate groups expands the polymer network. Due to the higher weight ratio of GEL in hydrogels, its effect on the degree of swelling was superior to NaCMC; hence, the maximum swelling was observed in acidic pHs (1.2, 5.5). Similar findings were presented by Khan and Taturo, and that the swelling ratio increases with increasing GEL content (Khan and Anwar 2021; Tataru et al. 2011). As shown in Table 2, hydrogels containing higher amounts of GEL (MN3) showed a higher degree of swelling than formulations containing lower amounts of gelatin (MN1, MN2). The swelling data of crosslinked hydrogels showed that by increasing the amount of GTA in the polymer hydrogel from 3.1 to 2.5 (wt/wt), the swelling decreases

significantly from 553 to 263%. This was owing to the hydrogel's mechanical strength increasing as a result of crosslinking and the formation of a more compact wall. Also, it is observed that MN5 has the highest GF with more crosslinker. Similar findings were reported that GF is directly related to crosslinking density (Khan and Anwar 2021). The GEL/NaCMC ratio of 5:1 showed a lower gel fraction compared to the ratio of 3:1 and 4:1. This is consistent with the results of Kreua-Ongarjnukool et al. (2020) who concluded that at constant concentrations of GTA, the gel fraction decreases with increasing polymer concentration, meaning that polymer chains have less crosslinking. Also, there was no significant difference between MN7 and MN6, indicating that the amount of drug did not affect GF. MN5 with the highest amount of GTA showed the lowest dissolution. Other authors have achieved similar results in examining the crosslinks of GEL/NaCMC (Khan and Anwar 2021; Favatela et al. 2021). They argued that increasing the crosslink density increases the mechanical strength of the hydrogel, which in turn leads to a decrease in the solubility of the hydrogel and reduces the water-uptake capacity of the polymer network. From data in Table 2, it is evident that the solubility at the 5:1 (MN3) ratio of polymers was higher than the ratio of 3:1 (MN1) which is in good agreement with the results of swelling. Similar findings were presented by Tataro et al. (Tataru et al. 2011) that as the amount of gelatin increased, more electrostatic repulsion was generated, leading to the relaxation of the polymer network. In MN3, MN6, and MN7 samples, the effect of drug amount on solubility was investigated. The MN7 sample showed the highest percentage of solubility. At a constant ratio of polymers and the amount of crosslinker, the solubility increases with the increasing amount of drug. This may be due to increased electrostatic repulsion between the polar groups of GEL and LidoHCl.

According to these results, during the first 10 min of release, a burst release effect was observed, and then, its value increased slightly for a while and was fixed after 60 min. Effects of various ratios of polymers in formulations MN1, MN2, and MN3 on release rates are presented in Fig. 8b. The MN3 formulation showed higher release rates than MN2. Similarly, MN2 revealed a higher release rate than MN1. Drug release experiments agreed with the study of swelling; as the rate of GEL versus NaCMC increases, the swelling increases, which in turn causes the higher release of drug (Fig. 8b). The effect of GTA content in MN3, MN4, and MN5 formulations on drug release rate is shown in Fig. 8a. The drug release rate was higher in the case of MN3 than in MN4 and MN5. This is because increasing the concentration of GTA leads to the formation of a rigid network structure. To elaborate the effect of drug loading on in vitro release profiles, three DMN samples (MN3, MN6, and MN7) were prepared with varying concentrations of LidoHCl (10, 20, and 40%) and kept the concentration polymers and GA constant. This indicates that an increase in drug concentration causes an increase in the release rates of drugs (Fig. 8c). Also, MN7 exhibited excellent antibacterial activity. According to previous studies, in the short contact time and low concentration of glutaraldehyde, the adverse effect on the skin does not remain (Ballantyne and Jordan 2001).

DMN array failure force is presented in Table 2. According to the literature, the insertion force required to overcome the barrier of the skin and deliver the drug efficiently into the skin is 0.058 (N needle^{-1}) (Davis et al. 2004). For MN3, MN4, and MN5 DMNs, failure force increased with an increasing amount of GTA. This dependence is expected because increasing the crosslinker quantity leads to a rigid network structure. Comparing the mechanical strength of neat GEL and GEL/NaCMC DMN arrays showed that the addition of NaCMC to GEL greatly increases the mechanical properties. However, pure GEL DMN arrays exhibit compression forces at the end (low stress at fracture) of 0.051 (N), while mechanical strength for GEL/NaCMC DMN arrays reached 0.162 ± 0.01 N. Liu et al. (2022) deduced that the addition of cellulose nanofibrils to GEL could effectively improve the strength and toughness of the composite hydrogels. They found that when the composite hydrogel is under stress, the load can be transferred efficiently between the GEL matrix and cellulose nanofibrils. As shown in Table 2, the mechanical strength of MN1 with a polymer ratio of 3:1 has higher mechanical strength than MN3 and MN2. However, there was no significant difference in the mechanical strength of various amounts of the drug (MN3, MN6, and MN7). The shape of the synthesized DMN before and after applying the force is shown in Fig. 5j and k.

Conclusion

Dissolving microneedles loaded lidocaine based on natural polymers GEL and NaCMC were synthesized using GTA as the crosslinking agent. Prepared DMN can replace conventional anesthetic delivery methods such as injections and topical creams, due to their dissolution in skin pH, rapid onset time, and ability to cross the SC layer and deliver the sufficient drug to the skin. FTIR was used to corroborate the formation of crosslinked hydrogels between GEL and NaCMC. Also, XRD analysis indicated that the LidoHCl remained crystalline in the hydrogels. In addition, the shape of the DMN was shown on scanning electron microscopy micrographs. The synthesized DMN showed excellent swelling and solubility at skin pH. The results of the drug release study demonstrated that it was

directly related to the ratio of polymers and the amount of drug and inversely to the amount of crosslinker. It was also observed that all samples presented a burst release in the first 10 min. Mechanical properties data revealed that all synthesized DMNs were able to cross the skin barrier. In this study, MN7 was considered the ideal DMN with the highest drug release rate and sufficient mechanical strength to penetrate the skin. It can be concluded that DMN loaded LidoHCl based on GEL/NaCMC hydrogels have the potential to be used as transdermal drug delivery devices. They can dissolve well in skin pH and are a good clinical tool in the field of local anesthesia and management of perioperative pain and chronic pain as well as before minor skin surgery, such as the removal of moles, warts, and verrucas.

Acknowledgements
Not applicable.

Authors' contributions
The authors read and approved the final manuscript.

Funding
No funding body has provided funding for this research.

Availability of data and materials
All data generated or analyzed during this study are included in this published article.

Declarations

Competing interests
The authors declare that they have no competing interests.

Author details
[1]Department of Polymer Engineering, Faculty of Engineering, Islamic Azad University, South Tehran Branch, P.O. Box: 11365/4435, Tehran, Iran. [2]Department of Polymer and Textile, Islamic Azad University, South Tehran Branch, P.O. Box: 11365/4435, Tehran, Iran. [3]Department of Polymer Processing, Iran Polymer and Petrochemical Institute (IPPI), P.O. Box: 14965-112, Tehran, Iran. [4]Department of Medical, Tehran Medical Sciences Branch Islamic Azad University, P.O. Box: 19395/1495, Tehran, Iran.

Received: 23 December 2022 Accepted: 27 February 2023
Published online: 03 April 2023

References

Abdellatif MK, Ibrahim TH (2020) Intraoperative infusion of lidocaine 2% reduces postoperative fentanyl requirements for pain control in renal transplantation surgery. Ain-Shams J Anesthesiol 12(1):1–6

Ahmad Z, Khan MI, Siddique MI, Sarwar HS, Shahnaz G, Hussain SZ, Bukhari NI, Hussain I, Sohail MF (2020). Fabrication and Characterization of Thiolated Chitosan Microneedle Patch for Transdermal Delivery of Tacrolimus. AAPS PharmSciTech 21(2):68. https://doi.org/10.1208/s12249-019-1611-9

Ali SM, Yosipovitch G (2013) Skin pH: from basic science to basic skin care. Acta Derm Venereol 93:261–267

Ballantyne B, Jordan SL (2001) Toxicological, medical and industrial hygiene aspects of glutaraldehyde with particular reference to its biocidal use in cold sterilization procedures. J Appl Toxicol 21:131–151. England

Bao Z, Xian C, Yuan Q, Liu G, Wu J (2019) Natural polymer-based hydrogels with enhanced mechanical performances: preparation, structure, and property. Adv Healthc Mater 8:1–11

Bello AB, Kim D, Kim D, Park H, Lee S-H (2020) Engineering and functionalization of gelatin biomaterials: from cell culture to medical applications. Tissue Eng Part B Rev 26:164–80. United States

Bonfante G, Lee H, Bao L, Park J, Takama N, Kim B (2020) Comparison of polymers to enhance mechanical properties of microneedles for bio-medical applications. Micro Nano Syst Lett 8(1):1–3. https://doi.org/10.1186/s40486-020-00113-0. Springer Singapore

Bos JD, Meinardi MMHM (2000) The 500 Dalton rule for the skin penetration of chemical compounds and drugs. Exp Dermatol 9:165–9. https://doi.org/10.1034/j.1600-0625.2000.009003165.x

Buhus G, Popa M, Desbrieres J (2009) Hydrogels based on carboxymethylcellulose and gelatin for inclusion and release of chloramphenicol. J Bioact Compat Polym 24:525–545

Cepeda MS, Tzortzopoulou A, Thackrey M, Hudcova J, Arora Gandhi P, Schumann R (2015) Adjusting the pH of lidocaine for reducing pain on injection. Cochrane Database Syst Rev 5:CD006581. pp 1–65

Cevc G, Chopra A (2016) Deformable (Transfersome®) vesicles for improved drug delivery into and through the skin. In: Percutaneous penetration Enhanc Chem methods penetration Enhanc. Springer, Berlin, Heidelberg. p 39–59. https://doi.org/10.1007/978-3-662-47862-2_3

Chen X, Yu H, Wang L, Wang N, Zhang Q, Zhou W et al (2021) Preparation of phenylboronic acid-based hydrogel microneedle patches for glucose-dependent insulin delivery. J Appl Polym Sci 138:1–11

Dash R, Foston M, Ragauskas AJ (2013) Improving the mechanical and thermal properties of gelatin hydrogels cross-linked by cellulose nanowhiskers. Carbohydr Polym 91:638–45. https://doi.org/10.1016/j.carbpol.2012.08.080. Elsevier Ltd.

Davis SP, Landis BJ, Adams ZH, Allen MG, Prausnitz MR (2004) Insertion of microneedles into skin: measurement and prediction of insertion force and needle fracture force. J Biomech 37:1155–1163

Devi N, Maji TK (2009) Preparation and evaluation of gelatin/sodium carboxymethyl cellulose polyelectrolyte complex microparticles for controlled delivery of isoniazid. AAPS PharmSciTech 10:1412–1419

Donnelly RF, Raj Singh TR, Woolfson AD (2010) Microneedle-based drug delivery systems: microfabrication, drug delivery, and safety. Drug Deliv 17(4):187–207. https://doi.org/10.3109/10717541003667798

Donnelly RF, Singh TRR, Garland MJ, Migalska K, Majithiya R, McCrudden CM et al (2012) Hydrogel-forming microneedle arrays for enhanced transdermal drug delivery. Adv Funct Mater 22:4879–4890. Wiley Online Library

Dugam S, Tade R, Dhole R, Nangare S (2021) Emerging era of microneedle array for pharmaceutical and biomedical applications: recent advances and toxicological perspectives. Futur J Pharm Sci 7:1–26. Future Journal of Pharmaceutical Sciences

Edgar AC-M, Guadalupe M-M, Gonzalo V (2021) Interactions of the molecular assembly of polysaccharide-protein systems as encapsulation materials. A review, Advances in Colloid and Interface Science, vol 295, ISSN 0001–8686. https://doi.org/10.1016/j.cis.2021.102398. https://www.sciencedirect.com/science/article/pii/S0001868621000397

Esteghlal S, Niakousari M, Hosseini SMH (2018) Physical and mechanical properties of gelatin-CMC composite films under the influence of electrostatic interactions. Int J Biol Macromol 114:1–9. https://doi.org/10.1016/j.ijbiomac.2018.03.079. Elsevier B.V.

Favatela F, Horst MF, Bracone M, Gonzalez J, Alvarez V, Lassalle V (2021) Gelatin/cellulose nanowhiskers hydrogels intended for the administration of drugs in dental treatments: study of lidocaine as model case. J Drug Deliv Sci Technol 61:101886. https://doi.org/10.1016/j.jddst.2020.101886. Elsevier B.V.

Ge S, Li M, Ji N, Liu J, Mu H, Xiong L et al (2018) Preparation of a strong gelatin-short linear glucan nanocomposite hydrogel by an in situ self-assembly process. J Agric Food Chem 66:177–186

Gomes C, Glass M, Kieffer J, Chiforeanu M, Philippe P (2016) Topical anaesthetic solutions for pain free suture of lacerations in the emergency Dr Sylvie Martus, Laurence Poncin • lacerations = frequent in a paediatric emergency room • usually: local anaesthesia by injection of Lidocaine – But: pain, fear and a

Gudin J, Nalamachu S (2020) Utility of lidocaine as a topical analgesic and improvements in patch delivery systems. Postgrad Med 132:28–36. https://doi.org/10.1080/00325481.2019.1702296. Taylor & Francis

Hajzamani D, Shokrollahi P, Najmoddin N, Shokrolahi F (2020) Effect of engineered PLGA-gelatin-chitosan/PLGA-gelatin/PLGA-gelatin-graphene three-layer scaffold on adhesion/proliferation of HUVECs. Polym Adv Technol 31:1896–1910

Han T, Das DB (2015) Potential of combined ultrasound and microneedles for enhanced transdermal drug permeation: a review. Eur J Pharm Biopharm. 89:312–28. https://doi.org/10.1016/j.ejpb.2014.12.020. Elsevier B.V.

Hao Y, Li W, Zhou X, Yang F, Qian Z (2017) Microneedles-based transdermal drug delivery systems: a review. J Biomed Nanotechnol 13:1581–1597
He X, Sun J, Zhuang J, Xu H, Liu Y, Wu D (2019) Microneedle system for transdermal drug and vaccine delivery: devices, safety, and prospects. Dose-Response 17:1–18
Houck CS, Sethna NF (2005) Transdermal analgesia with local anesthetics in children: review, update and future directions. Expert Rev Neurother 5:625–634. Taylor & Francis
Inamuddin A, Mohammad A (2018) Applications of nanocomposite materials in drug delivery
Ivone R, Yang Y, Shen J (2021) Recent advances in 3D printing for parenteral applications. AAPS J 23:87. https://doi.org/10.1208/s12248-021-00610-z
Jeong WY, Kwon M, Choi HE, Kim KS (2021) Recent advances in transdermal drug delivery systems: a review. Biomater Res 25:1–15. Biomaterials Research
Jesús P-P, Montserrat M-C, Dolors P-DM, Ramon T-GJ, Antonio B-M (2022) Release of ropinirole in acrylate transdermal patches: mutual interactions between formulation variables. AAPS PharmSciTech 23:82. United States
Khan S, Anwar N (2021) Gelatin/carboxymethyl cellulose based stimuli-responsive hydrogels for controlled delivery of 5-fluorouracil, development, in vitro characterization, in vivo safety and bioavailability evaluation. Carbohydr Polym 257:117617. https://doi.org/10.1016/j.carbpol.2021.117617. Elsevier Ltd
Kochhar JS, Lim WXS, Zou S, Foo WY, Pan J, Kang L (2013) Microneedle integrated transdermal patch for fast onset and sustained delivery of lidocaine. Mol Pharm 10:4272–4280. ACS Publications
Kochhar JS, Tan JJY, Kwang YC, Kang L (2019) Microneedle patch for fast onset and long-lasting delivery of painkillers. In: Microneedles Transdermal Drug Deliv. p 67–80
Kreua-Ongarjnukool N, Niyomthai ST, Sarodom K, Lothong T, Soomherun N (2020) Hybrid gelatin/carboxymethyl cellulose hydrogel loaded copper (II) ion for medical applications. Mater Sci Forum 1009 MSF:3–8
Krieger KJ, Bertollo N, Dangol M, Sheridan JT, Lowery MM, O'Cearbhaill ED (2019) Simple and customizable method for fabrication of high-aspect ratio microneedle molds using low-cost 3D printing. Microsystems Nanoeng 5(1):42. https://doi.org/10.1038/s41378-019-0088-8. Springer US
Kumar BK, Rajan VST, Begum NT (2012) Analytical method development and validation of lidocaine in ointment formulation by UV spectrophotometric method. Int J Pharm Pharm Sci 4:610–4. Available from: http://www.ijppsjournal.com/Vol4Issue2/3568.pdf
Lee B-M, Lee C, Lahiji SF, Jung U-W, Chung G, Jung H (2020) Dissolving microneedles for rapid and painless local anesthesia. Pharmaceutics 12:366. Multidisciplinary Digital Publishing Institute
Li W, Terry RN, Tang J, Feng MR, Schwendeman SP, Prausnitz MR (2018) Sustained release of a contraceptive. Nat Biomed Eng. Springer US. https://doi.org/10.1038/s41551-018-0337-4
Liu Q, Liu J, Qin S, Pei Y, Zheng X, Tang K (2020) High mechanical strength gelatin composite hydrogels reinforced by cellulose nanofibrils with unique beads-on-a-string morphology. Int J Biol Macromol 164:1776–84. https://doi.org/10.1016/j.ijbiomac.2020.08.044. Elsevier B.V.
Liu B, Yi X, Zheng Y, Yuan Z, Yang J, Yang J et al (2022) A review of nano/micro/milli needles fabrications for biomedical engineering. Chinese J Mech Eng (English Ed) 35(1):106. https://doi.org/10.1186/s10033-022-00773-6. Springer Nature Singapore
Ma G, Wu C (2017) PT NU SC. J Control Release. Elsevier B.V. https://doi.org/10.1016/j.jconrel.2017.02.011
Martell B, Kushner H, Richardson E, Mize A, Mayer P (2017) Pharmacokinetics of lidocaine and its metabolites following vaginal administration of lidocaine gel to healthy female subjects. Clin Pharmacol Drug Dev 6:27–35
Migdadi EM, Donnelly RF (2019) Microneedles for transdermal drug delivery. In: Imaging Technol. Transdermal Deliv. Ski. Disord
Mustafa Kamal NA, Tuan Mahmood TM, Ahmad I, Ramli S (2020) Improving rate of gelatin/carboxymethylcellulose dissolving microneedle for transdermal drug delivery. Sains Malays 49:2269–2279
Nayak A, Das DB, Vladisavljevi GT (2013) Microneedle-assisted permeation of lidocaine carboxymethylcellulose with gelatine co-polymer hydrogel
Nejad HR, Sadeqi A, Kiaee G, Sonkusale S (2018) Low-cost and cleanroom-free fabrication of microneedles. Microsystems Nanoeng 4:1–7. https://doi.org/10.1038/micronano.2017.73. The Author(s)
Nejad HR, Sadeqi A, Kiaee G, Sonkusale S (2018) Low-cost and cleanroom-free fabrication of microneedles. Microsyst Nanoeng 4:1–7. Nature Publishing Group
Pandit AP, Pol VV, Kulkarni VS (2016) Xyloglucan based in situ gel of lidocaine HCl for the treatment of periodontosis. J Pharm 2016:1–9
Pastore MN, Kalia YN, Horstmann M, Roberts MS (2015) Transdermal patches: history, development and pharmacology. Br J Pharmacol 172:2179–2209
Prausnitz MR, Langer R (2008) Transdermal drug delivery. Nat Biotechnol 26:1261–1268. Nature Publishing Group
Price R, Shur J, Ganley W, Farias G, Fotaki N, Conti DS et al (2020) Development of an aerosol dose collection apparatus for in vitro dissolution measurements of orally inhaled drug products. AAPS J 22:47. United States
Proksch E (2018) pH in nature, humans and skin. J Dermatol 45:1044–1052
Rasool A, Ata S, Islam A, Rizwan M, Azeem MK, Mehmood A et al (2020) Kinetics and controlled release of lidocaine from novel carrageenan and alginate-based blend hydrogels. Int J Biol Macromol 147:67–78. https://doi.org/10.1016/j.ijbiomac.2020.01.073. Elsevier B.V.
Roy G, Garg P, Venuganti VVK (2022) Microneedle scleral patch for minimally invasive delivery of triamcinolone to the posterior segment of eye. Int J Pharm 612:121305. https://doi.org/10.1016/j.ijpharm.2021.121305. Elsevier B.V.
Santos LF, Correia IJ, Silva AS, Mano JF (2018) Biomaterials for drug delivery patches. Eur J Pharm Sci 118:49–66. https://doi.org/10.1016/j.ejps.2018.03.020. Elsevier B.V.
Saraswathy K, Agarwal G, Srivastava A (2020) Hyaluronic acid microneedles-laden collagen cryogel plugs for ocular drug delivery. J Appl Polym Sci 137:1–14
Shah V, Choudhury BK (2017) Fabrication, Physicochemical Characterization, and Performance Evaluation of Biodegradable Polymeric Microneedle Patch System for Enhanced Transcutaneous Flux of High Molecular Weight Therapeutics. AAPS PharmSciTech 18(8):2936–2948. https://doi.org/10.1208/s12249-017-0774-5
Shin CI, Jeong SD, Rejinold NS, Kim Y-C (2017) Microneedles for vaccine delivery: challenges and future perspectives. Ther Deliv 8:447–60. Available from: https://www.future-science.com/doi/10.4155/tde-2017-0032
Spierings ELH, Brevard JA, Katz NP (2008) Two-minute skin anesthesia through ultrasound pretreatment and iontophoretic delivery of a topical anesthetic: a feasibility study. Pain Med 9:55–9. Available from: https://academic.oup.com/painmedicine/article-lookup/doi/10.1111/j.1526-4637.2007.00281.x
Tataru G, Popa M, Desbrieres J (2011) Microparticles of hydrogel type based on carboxymethylcellulose and gelatin for controlled release of water soluble drugs. Rev Roum Chim 56:399–410
USP38/NF33 (2015) Validation of compendial methods section. United State Pharmacopeial/National Formul, p 2256. The United States Pharmacopeial Convention 12601 Twinbrook Parkway, Rockville, MD 20852.
Vecchione R, Coppola S, Esposito E, Casale C, Vespini V, Grilli S et al (2014) Electro-drawn drug-loaded biodegradable polymer microneedles as a viable route to hypodermic injection. Adv Funct Mater 24:3515–3523
Vora D, Garimella HT, German CL, Banga AK (2022) Microneedle and iontophoresis mediated delivery of methotrexate into and across healthy and psoriatic skin. Int J Pharm 618:121693. https://doi.org/10.1016/j.ijpharm.2022.121693. Elsevier B.V.
Wagner H, Kostka KH, Lehr CM, Schaefer UF (2003) pH profiles in human skin: influence of two in vitro test systems for drug delivery testing. Eur J Pharm Biopharm 55:57–65
Wang M, Luo Y, Wang T, Wan C, Pan L, Pan S et al (2021) Artificial skin perception. Adv Mater 33:1–20
Xing Q, Yates K, Vogt C, Qian Z, Frost MC, Zhao F (2014) Increasing mechanical strength of gelatin hydrogels by divalent metal ion removal. Sci Rep 4:1–10
Xing M, Wang X, Zhao L, Zhou Z, Liu H, Wang B et al (2021) Novel dissolving microneedles preparation for synergistic melasma therapy: combined effects of tranexamic acid and licorice extract. Int J Pharm 600:120406. https://doi.org/10.1016/j.ijpharm.2021.120406. Elsevier B.V.
Xue X, Chen X, Mao X, Hou Z, Zhou Y, Bai H et al (2013) Amino-terminated generation 2 poly(amidoamine) dendrimer as a potential broad-spectrum, nonresistance-inducing antibacterial agent. AAPS J 15:132–142
Yang H, Kang G, Jang M, Um DJ, Shin J, Kim H et al (2020) Development of lidocaine-loaded dissolving microneedle for rapid and efficient local anesthesia. Pharmaceutics 12:1067. Multidisciplinary Digital Publishing Institute. Available from: https://www.mdpi.com/1999-4923/12/11/1067
Zempsky WT (2008) Pharmacologic approaches for reducing venous access pain in children. Pediatrics 122(Suppl 3):S140–S53

Zhang L, Guo R, Wang S, Yang X, Ling G, Zhang P (2021) Fabrication, evaluation and applications of dissolving microneedles. Int J Pharm 604:120749. https://doi.org/10.1016/j.ijpharm.2021.120749
Zhang L, Li Y, Wei F, Liu H, Wang Y, Zhao W, Dong Z, Ma T, Wang Q 2020 Transdermal Delivery of Salmon Calcitonin Using a Dissolving Microneedle Array: Characterization, Stability, and In vivo Pharmacodynamics. AAPS PharmSciTech 22(1):1. https://doi.org/10.1208/s12249-020-01865-z
Zhu Y, Carragher B, Potter CS (2001) Automated filament finding and selection from cryo electron micrographs. Microsc Microanal 7:986–987

Publisher's Note